High efficiency tin-based EUV sources

M. Richardson, C-S. Koay, C. Keyser, K. Takenoshita, E. Fujiwara[a] & M. Al-Rabban[b]
(Laser Plasma Lab, School of Optics & CREOL, University of Central Florida, Orlando, FL)
[a] Himeji University, Japan
[b] Qatar University, Qatar

ABSTRACT

We have previously proposed the use of mass-limited, tin-containing laser plasma sources for EUV lithography applications. Here we report advances in measurements of the spectral output, conversion efficiency, and debris emission from these sources. We also report progress in the use of repeller field debris inhibition techniques for this source.

Keywords: EUV sources, EUV lithography, mass-limited source, laser plasma,

1. INTRODUCTION

Providing a suitable EUV point source of sufficient power and longevity is one of the principal challenges facing the development of EUV lithography for fabricating future generation computer chips[1]. Both discharge and laser plasma sources are being developed to meet this need—a stable, debris-free, light source producing collectable in-band (2%) emission at ~13.5nm with power levels of ~100W[2]. For a laser plasma source to succeed in this application, it must operate continually for periods of ~1 year at repetition rate of 5-10 kHz with a pulse-to-pulse stability of < 2%. It must also function so that the large-NA (>0.25) collection optics do not suffer from the deleterious effects of target debris in long-term operation. The conversion efficiency from the laser light to useful EUV emission must be sufficiently large to (i) provide the projected required collectable power levels with viable commercial lasers and (ii) permit the overall cost of the source, including the laser, to remain within economic models of the overall EUV lithography stepper tool.

A number of laser plasma sources have been investigated for EUVL, including high density, pulsed or continuous cluster targets[3], liquid jets[4] or droplets[5] of liquid Xe, which emits broadband radiation (10-14nm from Xe^{9+} - Xe^{17+} ions), and water droplet[6] and jet[7] targets that radiate narrow line emission from Li-like O ions. Droplet targets have demonstrated extended operating lifetimes without significant debris contamination[8]. Both approaches showed conversion efficiencies to in-band radiation of <0.8% in 2π sr, a value that makes achieving the requirement for sufficient power for EUV lithography difficult with the available laser technology.

Here we look at some of the advantages of Sn-based plasma sources compared to Xe plasmas. The Xe and Sn laser plasmas source are compared and discussed for their EUV emission characteristics, based on a simulations made using the Cowan code. It is known that the emission at 13.5nm from Xe laser plasma sources is produced by emission predominantly from only the Xe^{10+} ions. Its principal UTA is located at 11nm, (Fig. 1(a)), with less than 5% of these ions emitting in the 13.5 nm region, and only half of these emitting within the 2% multi-layer mirror bandwidth. Since the maximum Xe^{10+} ion population in the plasma cannot exceed ~40%, it can therefore be argued that the conversion efficiency of the Xe source

Laser-Generated & Other Lab. X-Ray & EUV Sources, Optics, Apps., ed. G. A. Kyrala, J.-C. J. Gauthier, C. A. MacDonald, A. M. Khounsary, Proceedings of SPIE Vol. 5196 (SPIE, Bellingham, WA, 2004) · 0277-786X/04/$15 · doi: 10.1117/12.514083

from laser light to useful EUV cannot be expected to exceed much above 1% even when the Xe^{10+} ions are at their optimum plasma temperature.

A few steps away from Xe (atomic number Z = 54) on the periodic table is Sn (Z = 50). Moving from Xe to Sn, allows the principal UTA to move from 11nm to 13.5nm (Fig.1 (b)). Thus a tin plasma is inherently brighter than a Xe plasma. Moreover several of the adjacent Sn ion species (Sn^{7+} - Sn^{12+} emit at 13.5nm, and many of them contribute to the principal UTA at 13.5nm. Here we report the progress in

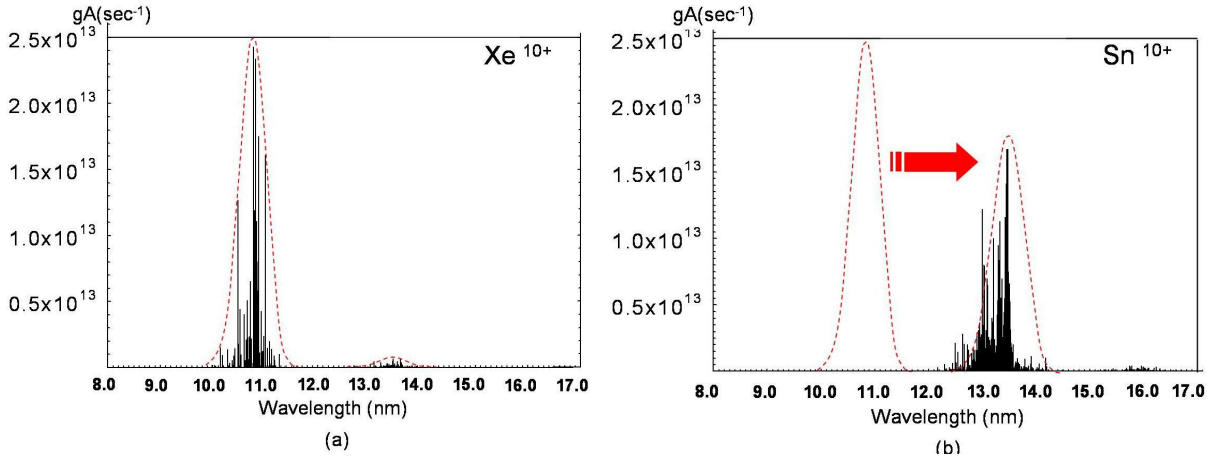

rve shows the principal UTA of Xe10+ ions located at 11nm. (b) The principal UTA shifts from 11nm to 13.5nm when changing from Xe to Sn.

our studies on a tin material[9-11] target. We demonstrate in-band conversion efficiencies in the range of ~ 2%, and describe our progress in minimizing plasma debris. These developments we believe will enable the generation of average EUV source powers > 60W of useful EUV source powers with current diode-pumped Nd:laser technology[12,13].

2. EXPERIMENTS AND RESULTS

Our approach to maximizing EUV conversion efficiency, and source repetition rate and minimizing target particulate debris is through the use of mass-limited targets. Here we define mass-limited as the minimum mass of a microscopic target that provides all the ions that radiate at the desired wavelength. We use a capillary dispenser to provide a thin train of 35-μm diameter droplets, each containing some tin, driven at a frequency of ~ 100-kHz (Fig. 2). The stability of droplets in the target region is about 3-μm and is synchronized to the laser with high precision (also ~ 3-μm). Not all the droplets are used in making plasma sources in the present setup, and the unused targets are collected in a cryogenically-cooled bucket.

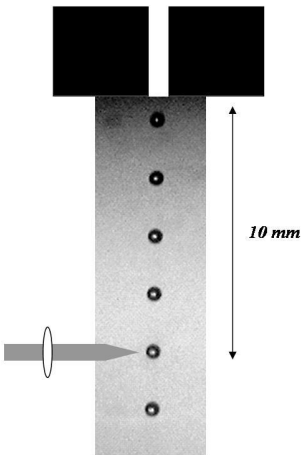

Figure 2: A train of droplet targets with a laser beam focused on a droplet.

A 5-cm focal length positive lens focuses the laser beam onto the droplet target to create laser plasma which produces EUV radiation. The focal spot size of the laser beam is less than 80-μm diameter and the irradiance at the focal spot can reach up to 10^{12} W/cm^2. The distance from the tip of the nozzle to the plasma is 10-mm. For

optimum coupling between the laser pulse and the target, all of the energy carried in the laser pulse should interact with the target.

Experiments are performed with the setup illustrated in Fig. 3. The target is located centrally in a 45-cm diameter vacuum chamber, which is operated at pressure below 10^{-3} Torr with a turbo-drag pump backed with a roughing pump. At this pressure, absorption of EUV radiation by the air inside the chamber is less than 1% for a distance from the plasma to the radiation detectors used for monitoring the EUV emission.

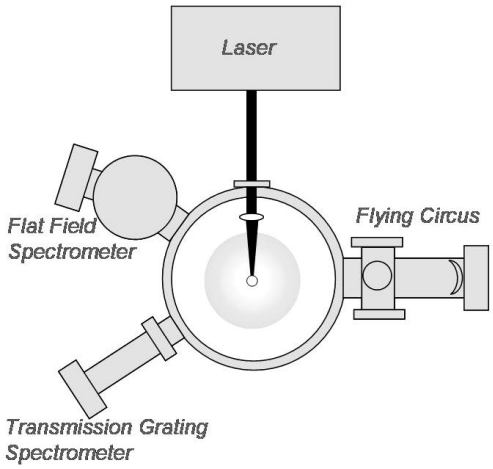

Figure 3: Target vacuum chamber for laser plasma source having various EUV diagnostics connected on different ports on the chamber.

Various diagnostics for studying the EUV radiation have been coupled to the ports on the chamber. High resolution spectra from the laser plasma emission have been obtained by using a flat-field reflection grating spectrometer and/or a transmission grating spectrometer. Each spectrometer can be connected to a back-thinned[14] x-ray CCD camera to record the dispersed spectrum.

The flat-field spectrometer (FFS) comprises of a 1200-lpm variable spaced reflective grating[15] in a configuration reported previously[16]. Light from the source passes through a 100-μm slit, through a Zr metal filter, incidents on the grating at a grazing angle, diffracts off the grating by reflection, and be detected on the CCD. The source-to-slit distance is 27-cm. The FFS has a linear spatial dispersion at the surface of the CCD, and thus the wavelength of the diffracted light recorded on the camera scales linearly with distance. The transmission grating spectrometer (TGS) has a 5000-lpm transmission grating. A 100-μm slit is placed between the source and the grating, with the same source-to-slit distance as in the FFS setup. The grating-to-CCD distance is 35-cm.

The EUV energy from the source is measured by using the Flying Circus (FC). The FC is aligned to the source at a 60 degree angle from the incident laser beam direction. A Mo-Si multilayer mirror in the FC that is used for collecting radiation from the source is located about 1-m from the source, subtending a 600-μsr collection solid angle. The FC is a portable EUV source diagnostic instrument[17]. It allows measurements of absolute EUV energy and average power as well as other characterization parameters of EUV source in the 13.5-nm region. The Mo-Si mirror has been calibrated with peak reflectivity at 13.5 nm and FWHM of 0.5 nm.

The laser used in these studies is a Q-switched Nd:YAG oscillator-amplifier laser system (output wavelength 1064-nm) that is capable of producing pulses with energy 1.6-J per pulse

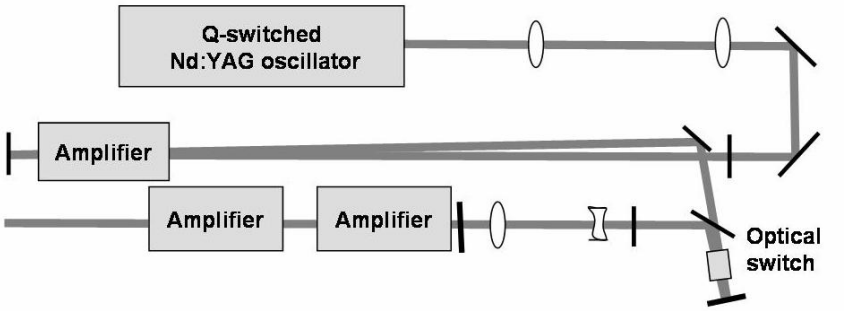

Figure 4: Schematic diagram of the layout of the 2Hz, 2 J, Q-switched Nd.YAG laser oscillator-amplifier system used for these studies

and pulse duration 10-ns at 2Hz repetition rate. The laser consists of a master oscillator and three amplifiers modules (Fig. 4). The laser beam has an $M^2 = 1.5$. Figure 5 shows the far field beam profile of the laser output at 1.6-J per pulse, and the temporal pulse shape of the laser beam.

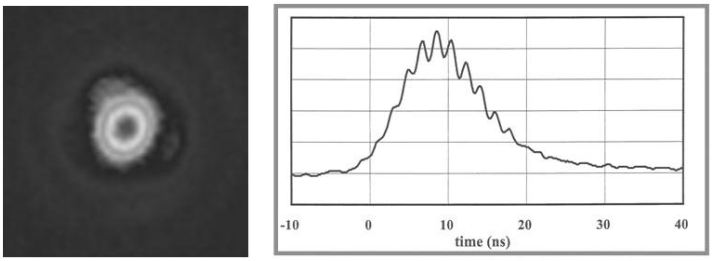

Figure 5: Laser beam cross-section and temporal pulse shape for pulse energy 1.6-J per pulse.

2.1 Spectral measurements and estimation of Conversion Efficiency

The diagnostics described above have been used for analyzing the spectrum of emission and conversion efficiency of the source. By using a 100-Hz 300-mJ 10-ns Nd:YAG laser (λ = 1064-nm), a spectrum of EUV radiation from the tin material laser plasma source was recorded using the FFS. For comparison, a spectrum for liquid water droplet source was also obtained. Fig.6 compares EUV spectra between both sources for the same number of laser shots.

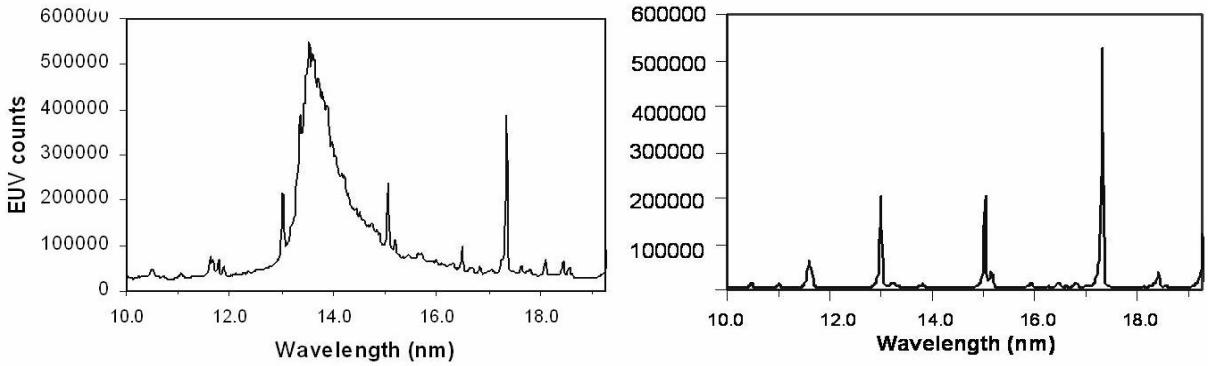

Figure 6: Comparison of the spectra recorded for tin material droplet source and water droplet source for the same

The spectrum from the water droplet source shows a narrow peak at ~ 13-nm corresponding to the 4d – 2p transition from Lithium-like Oxygen. In comparison, the spectral peak at 13-nm region for the tin material source is broader and higher than that of the water droplet source. This enhancement in the 13-nm emission for tin is made possible by the unresolved transition array (4d – 4f transitions) from Sn^{4+} to Sn^{13+} ions.

The amount of useful energy of EUV radiated from the laser plasma source is measured using the FC. The Mo-Si multilayer spherical mirror in the FC collects radiation from the laser plasma source and focuses the energy onto an AXUV–100 detector[18], which is a silicon p-n junction photodiode. The spectral responsivity of the detector at 13.5-nm is approximately 0.23A/W. The mirror reflectivity at normal incidence is taken to be 68% with a 3% spectral bandwidth centered at 13.5-nm. A 26-volt reversed bias is applied on the detector.

During the experiment, the FC was aligned to observe the plasma source at 60-degree angle from the incident laser beam. The distance from the plasma to the multilayer mirror was about 1-meter. A freestanding Zirconium metal filter of thickness 0.5-μm was placed in front of the detector to prevent any visible light from entering the detector, while allowing the 13.5-nm to pass with transmission of about 18%.

The EUV signal from the detector was observed with a high-speed oscilloscope connected to a 50-ohm terminator. The total EUV signal detected in 2π sr is determined from

$$E_{euv} = \frac{2\pi A_{scope}}{\Omega T_{filter} R_{mirror} S_{diode} Z_{scope}}$$

where Ω is the collection solid angle subtending a cone from the laser plasma to the multilayer mirror located in the FC, R_{mirror} and T_{filter} are the mirror reflectivity and metal filter transmission, S_{diode} is the spectral responsivity of the AXUV detector in A/W at 13.5nm, and Z_{scope} is the input impedance at the measurement channel into the oscilloscope. The integrated voltage of the EUV signal observed on the oscilloscope is A_{scope}. The conversion efficiency was measured to be 1.0% with the laser running at 1-Hz and pulse energy of 0.64-J. This value of conversion efficiency, however, is not the optimized value.

3. PLASMA HYDRODYNAMIC CODE CALCULATION

Radiation emitted from laser plasma depends strongly on the plasma conditions such as the electron temperature and electron density. The one-dimensional Lagrangian hydrodynamic code, MEDUSA, developed at Rutherford Laboratory[19], was used to model the hydrodynamic processes of the tin material target laser plasma. Calculations were made for a target with these parameters: 10% tin doped material, 35-μm diameter spherical target, 10-ns laser pulse duration and a 7.3 x 10^5W/sr laser intensity at the target. Fig.7. shows the electron temperature and density for a time when the peak of the laser pulse coincide with the center of the target.

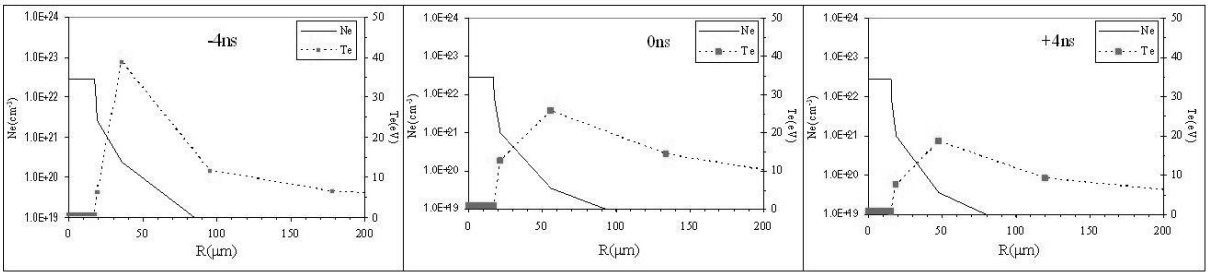

Fig. 6: Plots of electron temperature (*Te* in eV) and electron density (*Ne* in cm-3) as a function of distance from the center of target for a laser plasma of a tin doped target material. The time separation refers to the separation

4. OUT-OF-BAND EMISSION

Another concern in the design and development of high power 13.5 nm sources for lithography is the quantity of out-of-band EUV emission that is absorbed by the first and subsequent mirrors of the collector optics. As an illustration of the possible severity of this problem, Fig.8 shows the out-of-band emission from just the Sn^{10+} ion of tin-target plasma. It can be seen that this emission is several times greater than the in-band emission. This level of out-of-band emission will be magnified several-fold when the emission from other ions and target constituents are taken into account. With predicted in-band source requirements for a full-size stepper now being in the range of 500 W, the level of out-of-band emission absorbed by the first mirror (particularly) may be several kilowatts of power. Dissipating this heat will require careful attention to mirror design and materials. We are now embarking on a more rigorous investigation of the effects of out of band emission on the collector mirror.

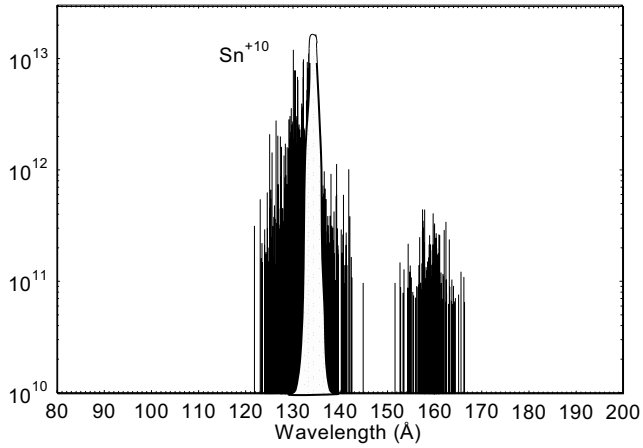

Figure 8: Code calculation of the emission of Sn^{10+} plotted on a logarithmic scale showing the amount of emission outside the acceptance window of a 2% bandwidth multilayer mirror at 13.5 nm.

5. DEBRIS STUDIES

Debris from the plasma source degrades the multi-layer mirror (MLM) reflectivity of the condenser optics. The overall lifetime of the combination of the plasma source and MLM optics depends mainly on how long the reflectivity of the first collimator mirror is maintained. It is a critical element in the system. This mirror is in direct line-of-sight of the source and sustains the full impact, not only of radiation outside the pass band of its coatings, but also of electrons, ions, neutral atoms and any particulate matter that originates directly from the target, or indirectly from other surfaces as a consequence of the source. All these factors can degrade the mirror in different ways. For instance, particulate matter, depending on its state, and kinetic energy, can coat, chip and/or indent the surface of the mirror. Ions, on the other hand will, with sufficient energy, ablate or sputter the coating layers, while oxygen atoms will tend to oxidize the uppermost silicon layer of the mirror, reducing its reflectivity.

Our approach to minimizing the effects of debris is through the use of mass-limited targets. Ideally we then have a source that consists of the absolute minimum number of radiating ions necessary to produce the required power. Since 1992, we have been investigating the use of microscopic liquid droplets at high repetition-rate as limited-mass laser plasma targets[5, 6]. We have previously made detailed lifetime studies of multilayer mirrors exposed to the long life effects of ions and particles from high repetition-rate (100 Hz) laser plasmas created from microscopic water droplet targets[20]. During this study, we developed several techniques that provide information on the progressive degradation of the mirror. We found, for instance, that Scanning Electron Microscopy (SEM) analysis of MLM's after this irradiation showed signs of sputtering by oxygen ions.

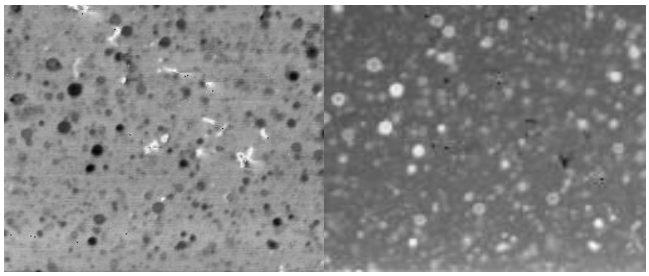

Figure 9: (a) AEM image 140mm X 140mm, (b) Back-scattered image (Same area)

In addition, if we slowed these ions down with a buffer gas, then X-ray Photoelectron Spectrometry (XPS) of the MLM's indicated oxidation of the mirror occurred. These studies also verified that MLM's sustained no detectable damage from particulate matter such as un-ionized chunks of material or even clusters when the water-droplet target was used as a source. This early work with water-droplet targets also led to the development of the repeller field concept of ion inhibition for debris mitigation[20].

Witness-plate post-shot analysis techniques as well as measurements of ions are used for debris analysis. The witness-plate post-shot analysis techniques can show direct result of the degradation caused by debris and the accumulated impact over a certain number of shots. Moreover, witness-plates can show the impacts caused by not only ions but also particulate matter which may not be charged at the time when the laser pulse and the target interact. Glass plates (microscope slides) and MLMs are the witness-plates in the current experiments. Measurement of ions can tell us about the ion velocity distributions and the species of ions. Charge collectors such as Faraday cup detectors and a Thomson parabola ion spectrometer are appropriate for such measurements.

Post-shot analysis of a witness-plate was carried out in the following manner. The laser used for the debris measurements and mitigation tests is a commercial (Spectra-Physics GCR-190) 100-Hz, 300-mJ, 10 ns, Q-switched Nd:YAG laser (1064- nm). The laser beam is focused to a spot size of 80-mm diameter onto the micro-targets by using a 50-mm focal length positive lens. Typical intensities at the focal spot are in the order of 10^{11} W/cm2. An MLM sample was exposed to the laser plasma source for 2.7 x 10^5 laser shots at a distance of 75-mm from the source. Fig. 9 shows an Auger Electron Microscopy (AEM) image and a back-scattered image. Both images show the same area of an MLM witness-plate surface. The back-scattered image shows the spatial distribution of high Z material, where the brighter spots are deposits of higher Z materials. The deposits shown in the AEM image completely overlapped the bright deposits on the back-scattered image. Since no signal of molybdenum was detected in Auger Electron Spectroscopy (AES), all the deposits must be tin.

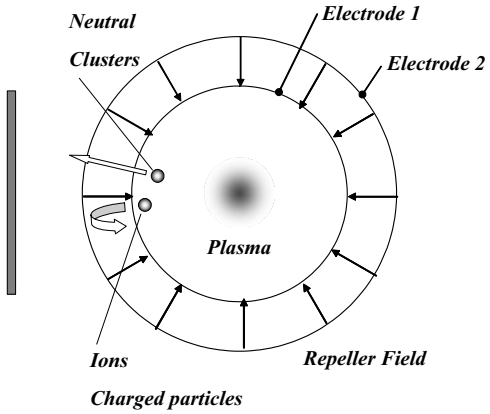

Figure 10: Schematic of repeller field concept.

5. A NEW REPELLER FIELD CONFIGURATION

The repeller field approach to debris mitigation was first applied to the water droplet target[20, 21]. We found that ion sputtering on the surface of the MLM was the cause for the drop of reflectivity of the mirror with progressive exposure to the source. The installation of a repeller electrostatic field between the source and the MLM, reduced considerably the ion flow, resulting in extended life of the mirror, by at least a factor of ~ 10.

We are now testing a more advanced version of this repeller field concept. The concept is shown in Fig. 10. Ions or charged particles will be repelled by the electric field established by the electrodes. Neutral clusters, however, are not affected by the field. They can pass through the field and deposit on the MLM surface.

The initial experiment for the repeller field was carried out under the following conditions. The diameter of the inner electrode is 27-mm and its potential is maintained at –100 V. The outer electrode is

42-mm in diameter and it is at 300-V potential. MLM samples are placed 30-mm away from the plasma source and at a 90 degrees angle of from the laser beam incident. The mirrors were exposed to the plasma source for a total of $3x10^4$ laser shots. The one of MLM samples for Auger Electron Microscopy (AEM) post-shot analysis was exposed to the plasma source with the repeller field and another one was without the field. By comparing the back -scattered images of the two MLM surfaces obtained by AEM analysis, it is found that less tin deposited on the MLM surface exposed to the plasma source with repeller field than the one without the field.

CONCLUSION

Our Sn-based droplet laser plasma source gave an initial value of conversion efficiency of 1.0% measured with the Flying Circus. Higher CE is possible with better pulse-and-target coupling and greater control of radiation dynamics. A combination of experimental and theoretical studies offers the best approach to designing the most optimum sources. Debris from laser plasmas produced from mass-limited targets is analyzed for the case of tin. A new repeller field configuration is examined and shown to have a marked effect on the flow of debris from the target.

ACKNOWLEDGMENTS

The authors gratefully acknowledge useful discussions with Dr. Gerard O'Sullivan from University College, Dublin, the technical support of colleagues at LPL, Dr. Greg Shimkaveg, Somsak Teerawattenasook, Joshua Duncan, and Rob Bernath, and wish to thank Drs David Attwood and Eric Gullickson from CXRO for multilayer mirrors. This work is supported by JMAR Technologies Inc., and the State of Florida.

REFERENCES

1. V.Y. Banine, J.P.H. Benschop, H.G.C. Werij, "Comparison of Extreme Ultraviolet Sources for Lithography Applications," *Microelectronic Eng.* 53, pp. 681-684, (2000)
2. C. Gwyn, D.Attwood, D. Sweeney, "Extreme Ultraviolet Lithography," *J. Vac. Sci. Technol. B* 16(6), pp.3142-3149, 1998
3. D.A. Tichenor *et al.,* "Diffraction-limited soft-x-ray projection imaging using a laser plasma source," *Opt. Lett.* **16**, 557 (1991)
4. B.A.M. Hansson, L. Rymell, M. Berglund, H.M. Hertz, "A liquid-xenon-jet laser-plasma X-ray and EUV source", *Microelectronic Eng.* **53**, 667 – 670 (2000)
5. D. Moyer, presented at Sematech Workshop on EUVL Source Development, San Jose, March 2, 2001 (unpublished)
6. F. Jin, K. Gabel, M. Richardson, M. Kado, A. F. Vassiliev & D. Salzmann, "Mass-limited laser plasma cryogenic target for 13 nm point x-ray sources for lithography," *Proc. SPIE*, vol. 2015, pp. 151-159, 1993.
7. M. Richardson, D Torres, C. DePriest, F. Jin, G. Shimkaveg, "Mass-limited, debris-free laser-plasma EUV source," *Optics Comm*., 145, pp. 109-112, (1998)
8. G. Schriever, M.Richardson & E.Turcu, (submitted for publication):
9. E. Turcu, H. Rieger, M. Powers, M. Richardson & C. Keyser (presented at Sematech Workshop on EUVL Source Development, Matsue Japan 2001 (unpublished))
10. first mentioned in a report by JMAR Research Corp.at the EUVL Source Workshop , March 2, 2001, Santa Clara, CA
11. patent pending
12. JMAR laser, diode-pumped 300W, 300Hz
13. TRW laser, diode-pumped Nd:YAG, 1700W, 5kHz

14. X-ray CCD camera model: MTE/CCD-1024-SB from Princeton Instrument
15. Concave diffraction grating (R = 5650-mm, size 26-mm x 46-mm) model: 001-0266 from HITACHI
16. W. Schwanda, K. Eidmann, and M.C. Richardson, "Characterization of a flat-field grazing-incidence XUV spectrometer," *J. X-ray Sci. and Tech*., vol. 4, pp. 8-17 (1993)
17. R. Stuik, F. Scholze, J. Tummler, and F. Bijkerk, "Absolute calibration of a multilayer-based XUV diagnostic," *Nuclear Inst. Method Phys. Res. A*, **429**, 305-316 (2002)
18. AXUV Series detectors from International Radiation Detectors Inc.
19. P.A. Rodgers, A.M. Rogoyski, and S. J. Rose, *MED101: a laser-plasma simulation code.* User guide (Appleton, Rutherford, N.J., 1989)
20. G. Shriever, M. Richardson & E. Turcu, The droplet laser plasma source for EUV lithography," *Proc. CLEO* 2000, p. 393-394 (2000)
21. M. Richardson and G. Schriever, US Patent 6,377,651, (2002).